REVIEW OF SCIENTIFIC INSTRUMENTS **85**, 045003 (2014)

Range-based control of dual-stage nanopositioning systems

Garrett M. Clayton,[1,a)] Christopher J. Dudley,[2] and Kam K. Leang[2,b)]
[1]*Department of Mechanical Engineering, Villanova University, Villanova, Pennsylvania 19085, USA*
[2]*Department of Mechanical Engineering, University of Nevada-Reno, Reno, Nevada 89557-0312, USA*

(Received 19 December 2013; accepted 30 March 2014; published online 17 April 2014)

A novel dual-stage nanopositioner control framework is presented that considers range constraints. Dual-stage nanopositioners are becoming increasingly popular in applications such as scanning probe microscopy due to their unique ability to achieve long-range and high-speed operation. The proposed control approach addresses the issue that some precision positioning trajectories are not achievable through existing control schemes. Specifically, short-range, low-speed inputs are typically diverted to the long-range actuator, which coincidentally has lower positioning resolution. This approach then limits the dual-stage nanopositioner's ability to achieve the required positioning resolution that is needed in applications where range and frequency are not inversely correlated (which is a typical, but not always the correct assumption for dual stage systems). The proposed range-based control approach is proposed to overcome the limitations of existing control methods. Experimental results show that the proposed control strategy is effective. © *2014 AIP Publishing LLC*. [http://dx.doi.org/10.1063/1.4870903]

I. INTRODUCTION

Nanopositioning systems are used in a broad range of instruments that are critical to the advancement of nanoscience, such as scanning probe microscope (SPMs), e.g., the atomic force microscope (AFM), the scanning tunneling microscope (STM), and related technologies. In many SPMs, there is a desire to achieve high-resolution positioning (nm-scale) over a large range (μm or larger) at high positioning speeds (e.g., to enable video-rate SPM[1]). Using conventional nanopositioning systems that use one actuator, these characteristics are not easily achievable because high resolution and speed typically require more compact and short range actuators.[2] Recently, dual-stage nanopositioning systems have gained significant interest because of their potential to achieve long-range, high resolution, *and* high-speed operation.[3–5]

A basic single-axis, dual-stage nanopositioner is depicted in Fig. 1. The system uses two actuators in each of the positioning axes, the first is a long-range, low-speed, lower-resolution actuator (long-range actuator, LRA) and the other a short-range, high-speed, high-resolution actuator (short-range actuator, SRA). In the setup from Fig. 1, the LRA is connected in series with a SRA to quickly and precisely position, for example, a SPM tool tip relative to a sample surface.[3–5]

There are a number of standard control algorithms employed to harness the unique characteristics of dual-stage systems.[6–9] These algorithms tend to split the control effort based on frequency, represented in Fig. 1 as complimentary (temporal) filters. Specifically, low-frequency inputs are applied to the low-speed LRA and high-frequency inputs are applied to the high-speed SRA. The use of this approach is predicated on the assumption that desired positioning range is inversely correlated to frequency and all inputs can be put into two categories: low-speed, long-range and high-speed, short-range, as illustrated in Fig. 2 (bottom-right and top-left, respectively)—note that this assumption is correct in some cases, for example, in dual-stage hard disk drive control where large-range, relatively low-frequency track seeks should be handled by the LRA and short-range, higher-frequency track following tasks should be handled by the SRA.

Although such a frequency-based approach enables tracking of both low and high frequency trajectories, one major challenge is that some precision positioning trajectories are not achievable. When using frequency-based approaches, short-range, low-speed inputs are diverted to the low-speed LRA, which results in lower positioning resolution. For example, standard piezo-stack actuators operate with a voltage range of 0–200 V regardless of positioning range. Assuming that the noise floor for a high-voltage amplifier is approximately 10 mV, then the positioning resolution for an actuator with a 20 micron stroke is 20 μm/200 V $\times$ 10 mV $=$ 1 nm. On the other hand, for an actuator with 1/10th of the range, the positioning resolution is 0.1 nm for the same amplifier noise floor. Therefore, LRAs have lower positioning resolution and should not be used for short-range, high-resolution operations, as would be necessary when imaging for nanofeature quality control.

To overcome this issue, this paper presents a novel method where control of dual-stage nanopositioners is achieved by considering spatial requirements, that is, range will be used to determine the allocation of control effort between the two actuators. This allows for low-speed, short-range inputs to be followed using the high-speed, higher resolution SRA, as shown in Fig. 2 (bottom-left). This is achieved through the use of a spatial filter which can be implemented on-line. The remainder of this paper is devoted to the development and experimental implementation of this range-based dual-stage control strategy.

a)Electronic mail: garrett.clayton@villanova.edu
b)Electronic mail: kam@unr.edu

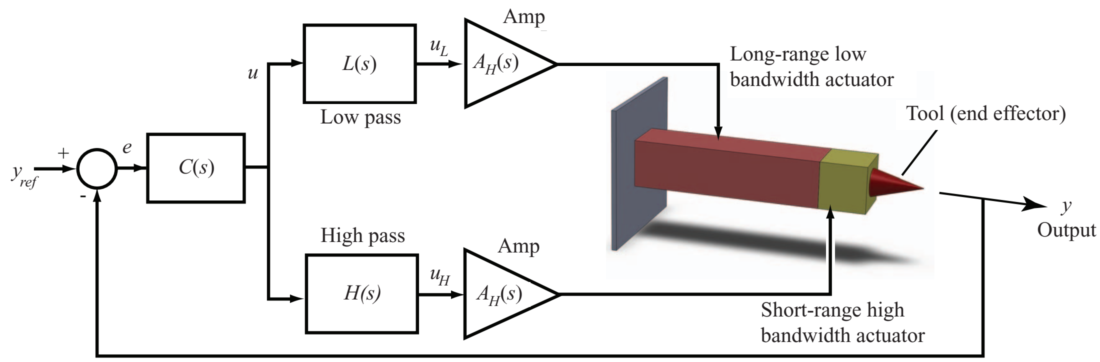

FIG. 1. A typical single-axis, dual-stage nanopositioner, and typical feedback control system.

II. RANGE-BASED CONTROL STRATEGY

A block diagram of the range-based control scheme implemented in this paper is shown in Fig. 3—note that the two actuators in the system, G_1 and G_2, are controlled separately using the feedback controllers, C_1 and C_2. The key innovation associated with the proposed control algorithm is the spatial filter which is used to allocate the control effort (based on range) for the dual-stage system represented by G_1 and G_2. Specifically: (1) short-range inputs at any frequency should be assigned to the high-speed, high-resolution SRA—dark grey region in Fig. 2 and (2) long-range, low-frequency inputs should be assigned to the low-speed LRA—light grey region in Fig. 2.

A. Spatial filtering approach

The spatial filter, shown in the block diagram in Fig. 3, consists of three primary components:

1. Manipulation: The original desired trajectory y_d, is manipulated to expose spatial information, resulting in a new signal $y_{d,\,r}$.
2. Filtering: The spatial information $y_{d,\,r}$ is filtered, resulting in two signals—one corresponding to long range components $y_{d,\,r,\,1}$ and one corresponding to short range components $y_{d,\,r,\,2}$.
3. Reconstruction: Long and short range signals $y_{d,\,1}$, $y_{d,\,2}$ are recovered from the two spatial signals.

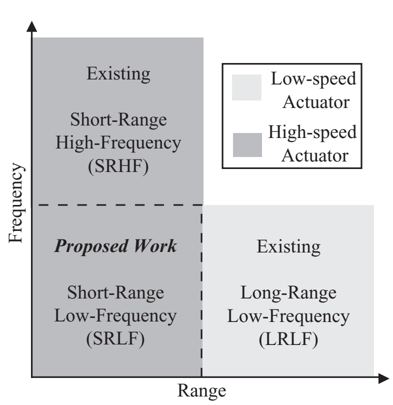

FIG. 2. The contributions of the proposed work towards advancing the state-of-the-art.

1. Manipulation

In order to split the temporal desired trajectory y_d into long and short range components, it needs to be manipulated to expose the trajectory's spatial information. Furthermore, it is advantageous to have the signal expose the spatial information in the form of spatial frequency, i.e., long range components appear at a low spatial frequency and short range components appear at a high spatial frequency, thus facilitating the use of standard filtering techniques. To achieve this, the signal y_d is plotted versus the total change in desired trajectory,

$$\sigma[n] = \sigma[n-1] + |y_d[n] - y_d[n-1]|, \tag{1}$$

with $\sigma[0] = 0$.

An example of the signal manipulation is shown in Fig. 4. In (a) two input sinusoids having the same frequency (1 Hz), but different amplitudes (0.5 and 2) are plotted versus time. Note that if these signals were split solely based on frequency (i.e., using complementary low-pass and high-pass temporal filters) both input signals would pass through the same filter and not be split. In (b), these same signals are plotted versus the total change in desired trajectory from Eq. (1). In this case, the resulting signals have different spatial frequencies (high spatial frequency corresponds to short-range and low spatial frequency corresponds to long-range). If these signals were now passed through complementary filters, provided the cutoff frequency is chosen properly, the signals would be assigned to different ranges, and thus, different actuators. In (c) and (d) signals of different frequencies (1 Hz and 10 Hz), but the same amplitude (0.5) are plotted versus time (c) and the cumulative sum (d). In this case, although the signals have

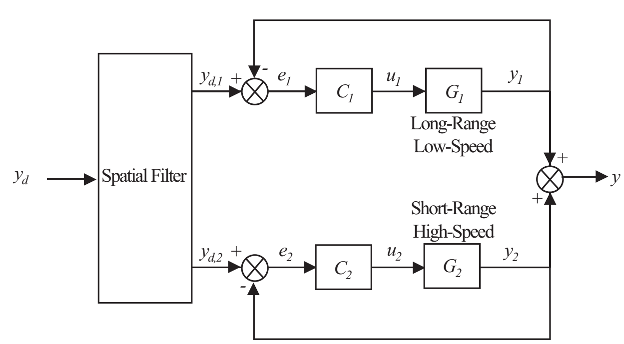

FIG. 3. Range-based control scheme.

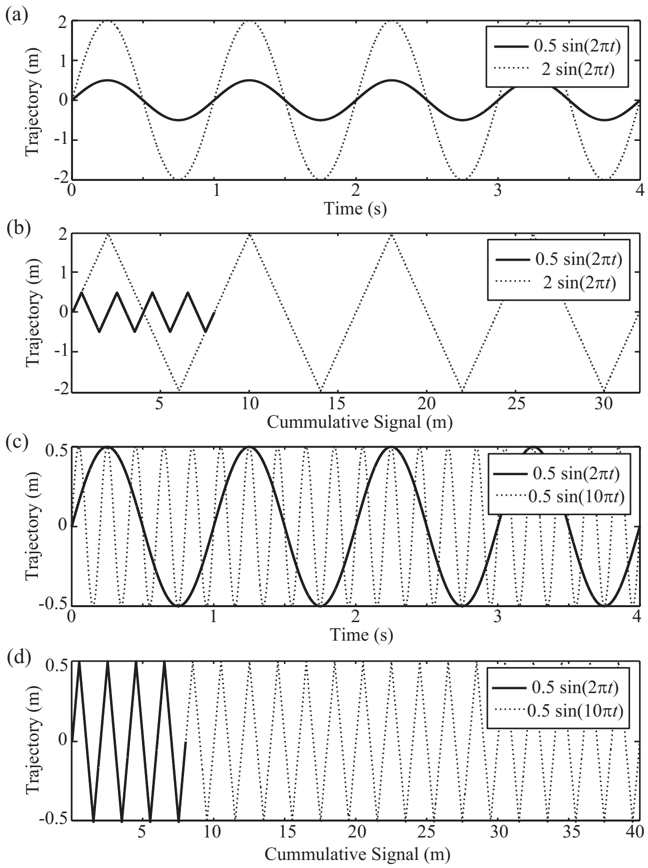

FIG. 4. Example of how the signal can be manipulated to highlight range (see (b) and (d)) as opposed to frequency (see (a) and (c)).

different frequencies in the time domain, they have the same spatial frequency.

2. Filtering

The manipulated signal $y_{d,\,r}$ is now passed through complementary filters (i.e., low-pass and high-pass) to split the range. The difference equations corresponding to these filters, which were developed by designing equivalent analog filters and then digitizing them using Tustin's method, are

$$y_{d,r,1}[n] = -\frac{\pi f_{co} D_n - 1}{\pi f_{co} D_n + 1} y_{d,r,1}[n-1] + \frac{\pi f_{co} D_n}{\pi f_{co} D_n + 1}(y_{d,r}[n] + y_{d,r}[n-1]) \quad (2)$$

and

$$y_{d,r,2}[n] = -\frac{\pi f_{co} D_n - 1}{\pi f_{co} D_n + 1} y_{d,r,2}[n-1] + \frac{1}{\pi f_{co} D_n + 1}(y_{d,r}[n] - y_{d,r}[n-1]), \quad (3)$$

where the subscripts 1 and 2 denote the long and short range signals, respectively, f_{co} is the spatial cutoff frequency in cycles per distance, and $D_n = |y_d[n] - y_d[n-1]|$ is the sampling distance (similar to sampling time). These filters are identical to typical temporal filters with two exceptions. First, for a given cutoff range R_{co} (2 times the cutoff signal amplitude), the spatial cutoff frequency is $f_{co} = \frac{1}{2R_{co}}$. The 2 in the denominator occurs because 1 cycle of the signal covers a distance $2R_{co}$. Second, the sampling distance D_n is not constant. This necessitates the recalculation of the filter parameters for each step, which can be implemented on-line without significant lag. The time varying nature of the filter parameters must be considered if the filters were placed in the control loop (e.g., as shown in Fig. 1). In the implementation considered in this paper, Fig. 3, they are outside the closed loop and thus, do not affect stability.

An example of this complementary filtering process is shown in Fig. 5 for a 1 Hz sinusoidal trajectory. The manipulated input signals $y_{d,\,r}$ on the left are passed through the complementary filters designed to have a cutoff range of $R_{co} = 10$, and thus, a spatial frequency of $f_{co} = \frac{1}{20}$. Each of the three signals represents different desired trajectory y_d ranges,

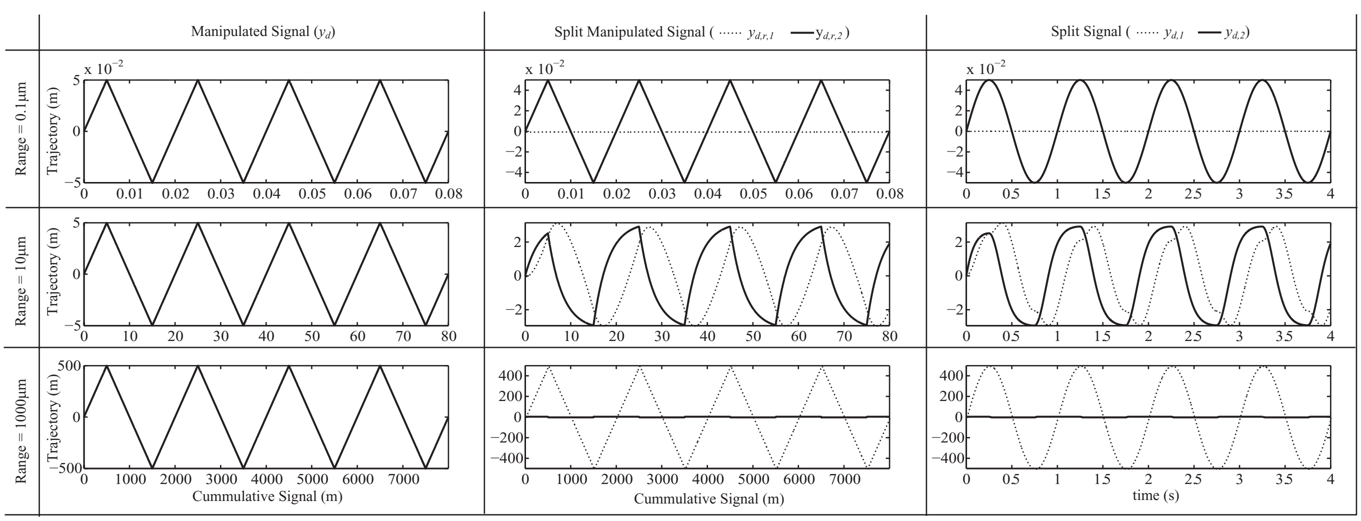

FIG. 5. Example of the spatial filtering process with range cutoff of 10 μm for three different range signals (0.1 μm—top, 10 μm—middle, and 1000 μm—bottom). Signals shown (from left to right) are the manipulated signal, the split manipulated signal, the split signal.

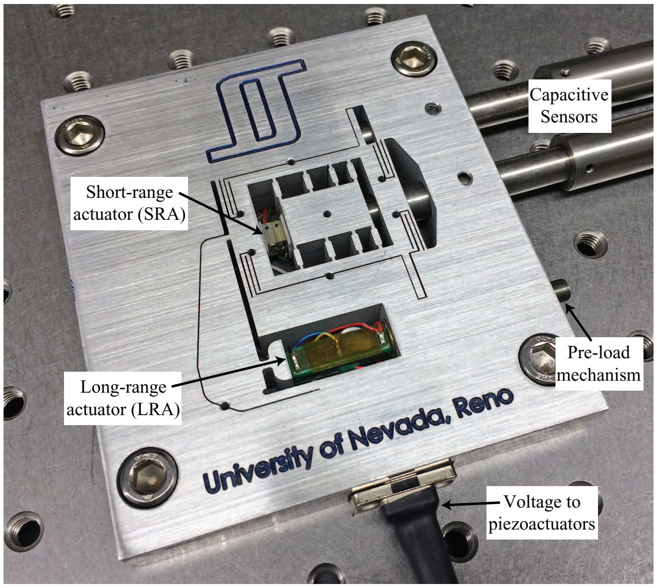

FIG. 6. Custom-designed single-axis dual-stage nanopositioner.

specifically the top has range $R = 0.1$, the middle has range $R = 10$, and the bottom has range $R = 1000$. In the first case (top), the range is small relative to the cutoff range $R = 0.1 \ll R_{co}$, the spatial filter results in most of the signal being passed to the SRA $y_{d,\,r,\,2}$. In the bottom case, where the range is long relative to the cutoff range $R = 1000 \gg R_{co}$, the filters result in most of the signal being passed to the LRA $y_{d,\,r,\,1}$. In the middle case, where the range is equal to the cutoff range $R = 10 = R_{co}$, both the long range $y_{d,\,r,\,1}$ and short-range $y_{d,\,r,\,2}$ signals have similar amplitudes. These results show that the desired trajectory y_d is split between the two actuators based on range.

3. Reconstruction

Given the split signals $y_{d,\,r,\,1}$, $y_{d,\,r,\,2}$ the long and short range temporal signals are recovered by replotting the spatial signals versus time. An example of this is shown in Fig. 5. The split signals (middle column) are replotted versus time as shown on the right, yielding the split temporal signals $y_{d,\,1}$, $y_{d,\,2}$. Note that if added together, the two signals equal the original input $y_d = y_{d,\,1} + y_{d,\,2}$ with little error (not shown).

TABLE I. Poles and zeros for the experimental dual stage system. Note: $i = \sqrt{-1}$.

	LRA G_1	SRA G_2
Gain (K)	3.06×10^{10}	5.91×10^{11}
Poles (p_i)	$-10.539 \pm 1407.9i$	$-966.6 \pm 14216i$
	-5000	$-8.812 \pm 1420.2i$
		-20736
Zeros (z_i)	N/A	$-7.1561 \pm 1837i$

III. EXPERIMENTAL VALIDATION

Experiments on a custom piezoelectrically driven dual-stage nanopositioner were carried out to validate the control strategy. The overarching goal of the following experiments is to show the feasibility of the proposed range-based dual-stage system control strategy. Subgoals include: (1) showing that the spatial filter can be implemented on-line and (2) validating the control system presented in Fig. 3.

A. Dual-stage system

The dual-stage system used in the following experiments is shown in Fig. 6. The two actuators are connected in series, as illustrated previously in Fig. 1. The range of the LRA is ± 9 μm and the range of the SRA is ± 0.6 μm. The system frequency response (including the amplifiers used to drive the piezoactuators) was characterized using a dynamic signal analyzer (Stanford Systems SR785) and a laser vibrometer (Polytec CLV 700). Frequency response plots for each stage are shown in Fig. 7 with the dashed line representing the raw frequency response data and the solid line representing the developed models.

The developed models are of the form

$$G(s) = K\,\frac{\prod_{i=1}^{m} s - z_i}{\prod_{j=1}^{n} s - p_j}, \tag{4}$$

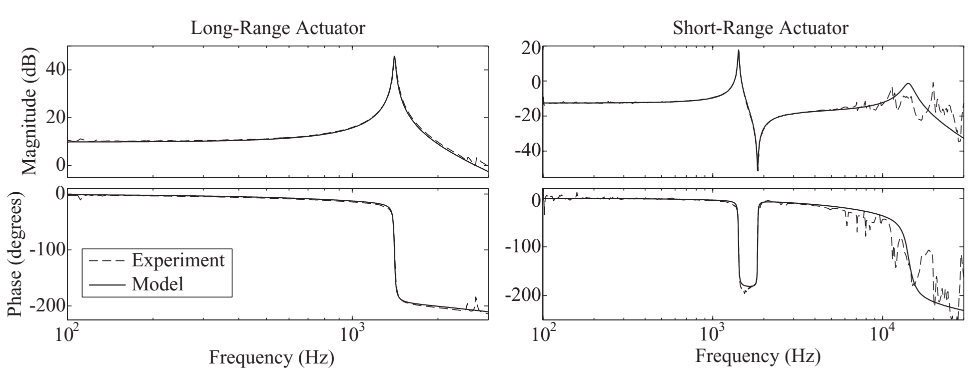

FIG. 7. Frequency response plots for the LRA (left) and the SRA (right).

where s is the Laplace variable, K is a gain, z_i is one of m zeros, and p_i is one of n poles. Specific values of each of the actuators is shown in Table I.

B. Spatial filter

The spatial filter was implemented on-line using the dual-stage positioner, capacitive sensors (ADE Technologies Microsense) to measure the position, and a MyDAQ data acquisition card programmed using LabVIEW. Using the complementary filters from Eqs. (2) and (3), a ramped sinusoid,

$$y_d = \frac{4t}{100}\sin(1/20\pi t), \tag{5}$$

shown in Fig. 8 (top), was spatially filtered. Given the ranges of the two actuators, a range cutoff of $R_{co} = 1\ \mu$m was chosen. Results from this experiment are shown in Fig. 8 (bottom).

Inspection of the split signals yields the following thoughts:

1. The crossover between the two actuators occurs when the range of the desired trajectory (dotted line) goes above the range cutoff $R_{co} = 1\ \mu$m at approximately 20 s into the trajectory. Below the range cutoff, the trajectory is diverted primarily to the short-range actuator, at the cutoff, the trajectory is split between the two actuators, and above the cutoff, the trajectory is increasingly diverted to the long-range actuator.
2. It is clear that above the range cutoff, the entire trajectory is not diverted to the long-range actuator. There are two reasons for this. First, the spatial filters used in the simulation are first order, and therefore do not completely attenuate the effect of large-range signals on the short-range actuator. Second, when the signal is manipulated to expose the spatial frequency, the signal is no longer sinusoidal (e.g., see Fig. 4). This trajectory contains higher frequency components, which correspond to short-range signals.

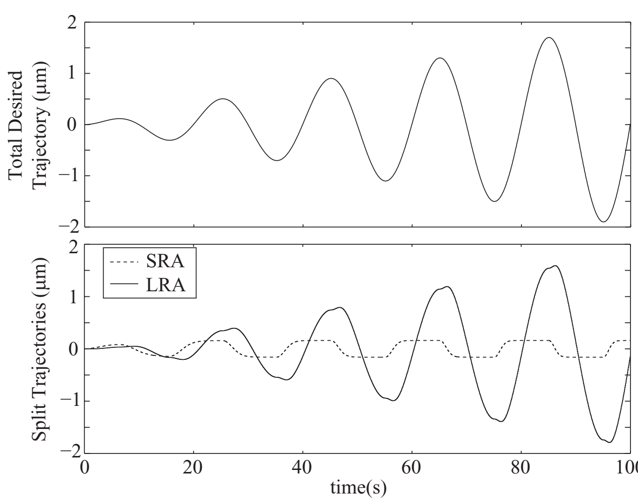

FIG. 8. Range splitting example, showing the desired trajectory (top) and the two split trajectories for the SRA (dashed line) and the LRA (solid line).

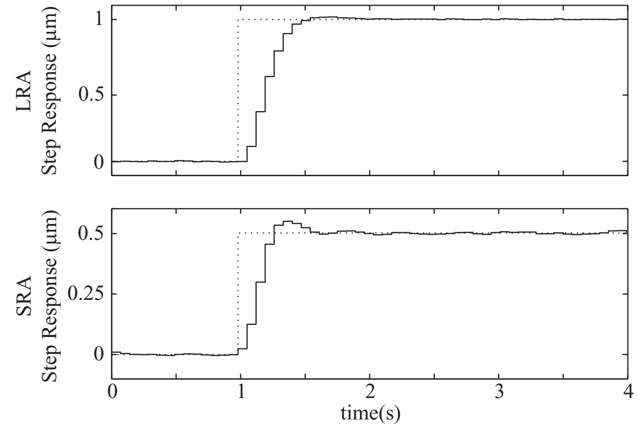

FIG. 9. Closed loop step response of the LRA (top) and the SRA (bottom).

C. Controller design

One of the advantages of the presented method is that the controller design problem is completely decoupled, that is, the LRA and SRA controllers can be designed separately. This significantly simplifies controller design when compared to methods where the controllers must be co-designed. It should be noted that any number of controllers can be used to control the two actuators.[2,10–13]

In this work, proportional-integral-derivative (PID) type controllers were designed in continuous time using root locus analysis and digitized using Tustin's method, yielding the following digital controllers:

$$C_{LRA} = \frac{0.0461z^2 + 0.0822z + 0.0366}{z^2 - 0.444z - 0.556} \tag{6}$$

and

$$C_{SRA} = \frac{1.2540z^2 + 2.4812z + 1.2313}{z^2 + 0.0005z + 0.9995}. \tag{7}$$

Figure 9 shows the closed loop step response for both actuators (top—LRA and bottom SRA). Both actuators achieve a closed loop settling time of approximately 0.5 s.

D. Experimental results and discussion

The trial trajectory, shown at the top of Fig. 10 as a dashed line, is a large-range 3 μm pulse plus a short-range sinusoidal signal, $0.2\sin(2\pi t)$. This trajectory has been chosen to highlight the advantages of the presented control method. As can be seen in Fig. 7, the LRA has a bandwidth of approximately 1 kHz, while the SRA has a bandwidth of approximately 10 kHz (ignoring the actuator cross coupling at 1 kHz). If frequency-based control allocation techniques were used, the trajectory would be split at around 1 kHz—this would result in the LRA handling the entire trajectory. In contrast, if using range-based allocation with a range cutoff of $R_{co} = 1\ \mu$m, the large-range pulse should be handled by the LRA and the short-range sinusoid should be handled by the SRA.

Figure 10 shows experimental range-based control results for the desired trajectory discussed above. Shown in this figure are the entire trajectory followed by the dual-stage

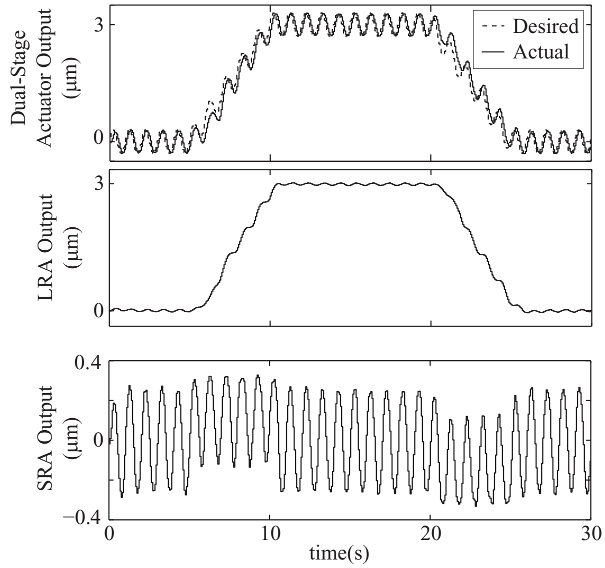

FIG. 10. Experimental range-based dual-stage control results, showing the desired and actual trajectories (top), the actual LRA trajectory (middle) and the actual SRA trajectory (bottom).

system (top, solid line), the trajectory followed by the LRA (middle), and the trajectory followed by the SRA (bottom). From these results, the presented range-based control algorithm is validated, as the spatial filter is able to separate the large-range pulse (primarily handled by the LRA—middle) from the short-range sinusoid (primarily handled by the SRA) and the designed controllers are able to track the desired trajectory.

[1] B. J. Kenton and K. K. Leang, "Design and control of a three-axis serial-kinematic high-bandwidth nanopositioner," IEEE/ASME Trans. Mechatronics **17**(2), 356–369 (2012).

[2] G. M. Clayton, S. Tien, K. K. Leang, Q. Zou, and S. Devasia, "A review of feedforward control approaches in nanopositioning for high speed SPM," ASME J. Dyn. Syst. Meas. Control **131**(6), 061101 (2009).

[3] B. J. Kenton, A. J. Fleming, and K. K. Leang, "A compact ultra-fast vertical nanopositioner for improving SPM scan speed," Rev. Sci. Instrum. **82**, 123703 (2011).

[4] G. Schitter, W. F. Rijkee, and N. Phan, "Dual actuation for high-bandwidth nanopositioning," in *47th IEEE Conference on Decision and Control, 2008. CDC 2008* (IEEE, 2008), pp. 5176–5181.

[5] A. J. Fleming, "Dual-stage vertical feedback for high speed-scanning probe microscopy," IEEE Trans. Control Syst. Technol. **19**(1), 156–165 (2011).

[6] T. Semba, T. Hirano, J. Hong, and L.-S. Fan, "Dual-stage servo controller for hdd using mems microactuator," IEEE Trans. Magn. **35**(5 Pt 1), 2271–2273 (1999).

[7] R. Horowitz, Y. Li, K. Oldham, S. Kon, and X. Huang, "Dual-stage servo systems and vibration compensation in computer hard disk drives," Control Eng. Pract. **15**(3), 291–305 (2007).

[8] S. J. Schroeck, W. C. Messner, and R. J. McNab, "On compensator design for linear time-invariant dual-input single-output systems," IEEE/ASME Trans. Mechatronics **6**(1), 50–57 (2001).

[9] D. Iamratanakul, B. Jordan, K. K. Leang, and S. Devasia, "Optimal output transitions for dual-stage systems," IEEE Trans. Control Syst. Technol. **16**(5), 869–881 (2008).

[10] S. Devasia, E. Eleftheriou, and S. O. R. Moheimani, "A survey of control issues in nanopositioning," IEEE Trans. Control Syst. Technol. **15**(5), 802–823 (2007).

[11] S. Salapaka, A. Sebastin, J. P. Cleveland, and M. V. Salapaka, "High bandwidth nano-positioner: a robust control approach," Rev. Sci. Instrum. **73**(9), 3232–3241 (2002).

[12] U. Aridogan, Y. Shan, and K. K. Leang, "Design and analysis of discrete-time repetitive control for scanning probe microscopes," ASME J. Dyn. Syst. Meas. Control **131**, 061103 (2009).

[13] K. K. Leang, Q. Zou, and S. Devasia, "Feedforward control of piezoactuators in atomic force microscope systems: Inversion-based compensation for dynamics and hysteresis," IEEE Control Syst. Mag. **29**(1), 70–82 (2009).